Foods and Raw Materials. 2027;15(1)

ISSN 2308-4057 (Print)
ISSN 2310-9599 (Online)

Research Article
Open Access

Available online at http://jfrm.ru/en
https://doi.org/10.21603/2308-4057-2027-1-702
https://elibrary.ru/XFWACU

Hydraulic lobe-pump inter-operational transportation of cheese spreads

Natalya R. Akhmedova[1,*], Oksana I. Levicheva[1,2], Vladimir A. Naumov[1]

[1] Kaliningrad State Technical University, Kaliningrad, Russia
[2] Baltfarmatsevtika LLC, Bagrationovsk, Russia

* e-mail: isfendi@mail.ru

Received 28.03.2025; Revised 06.05.2025; Accepted 13.01.2026; Published online 20.04.2026

Abstract:
When pumped from one production unit to another, molten cheese spread is a highly viscous liquid, which inevitably affects all hydraulic calculations for optimal pipeline characteristics. However, such calculations often miss out the effect of the viscosity on the pump efficiency. This article introduces a new method for determining the optimal pipe diameter to transport liquid media during food production. It takes into account the viscosity of the liquid and the technical characteristics of the rotary lobe pump.
The research featured a lobe-pump hydraulic system for transporting highly viscous cheese spreads. The calculations involved the technical parameters of the lobe pump and pipelines, as well as electricity tariffs. To determine the annual electricity costs, we used electricity tariffs for small businesses as of June 2024 in three random regions of the Russian Federation. The parameters of different cheese spreads (55–95°C) came from scientific publications in the public domain.
Among the various factors that affected the optimal pipe diameter, the greatest impact belonged to the temperature-related changes in viscosity. As the operation time of the lobe pump increased, so did the share of electrical energy costs. As a result, the optimal diameter of the pipeline increased significantly to compensate for the hydraulic pressure losses and energy costs. The optimal diameter also depended on the investment parameters. Bigger Life-Cycle values correlated with larger optimal pipe diameters, i. e., the reduced costs went down. Higher interest rates, on the other hand, correlated with smaller optimal pipe diameters, i. e., the reduced costs went up. In general, the overall efficiency of the pumping station depended quite strongly on all the factors featured in this research.
The new method made it possible to determine the optimal pipe diameter for inter-operational transportation of cheese spreads in particular and highly viscous laminar fluids in general. It relied on viscosity values and lobe pump specifications. Numerically, it was based on a step-by-step calculation of economic and hydraulic parameters. The method demonstrated good prospects for food pipeline design.

Keywords: Rotary pump, lobe pump, cheese spread, hydraulic system, optimal pipe diameter, viscosity, pipe efficiency

Funding: The research was part of a State R&D Assignment on innovative food engineering processes.

Please cite this article in press as: Akhmedova NR, Levicheva OI, Naumov VA. Hydraulic lobe-pump inter-operational transportation of cheese spreads. Foods and Raw Materials. 2027;15(1):184–194. https://doi.org/10.21603/2308-4057-2027-1-702

INTRODUCTION

Cheese spread being a popular dairy product, its physicochemical properties and production methods are a popular research topic [1–5]. The problem is that pumping liquid components and finished cheese spreads requires a lot of energy. As a result, food scientists are on the lookout for advanced food spread production technologies with greater efficiency and lower energy costs [6–9].

Hydraulic calculations usually make it possible to improve the pipeline performance. However, such calculations tend to ignore the properties of the pump. For example, Stoforos & Simunovic [10] used computational fluid dynamics to compare two flow patterns for a sweet potato puree unit. The first pattern involved a conventional shell-and-tube heat exchanger for cooling down viscous products. The second pattern featured an annulus of a tube-in-tube heat exchange, where the sweet potato puree flew within the annulus and the inner tube. As the flow was considered stationary and laminar, the mathematical model was represented as a system of Navier–Stokes equations for non-isothermal fluid flow. The stress, Pa, was determined as $\tau = K \times \omega^m$, where ω is the shear rate. Empirical coefficient (K) and exponent (m)

are determined experimentally for 25–95°C. The claimed power economy of the tube-in-tube heat exchanger was 25%. Although the puree supply into the heat exchanger was continuous, Stoforos & Simunovic ignored the properties of the pump that were bound to change due to the growing hydraulic resistance in the pipes.

Genereaux [11] was the first to solve the optimal diameter problem for straight pipelines. On the one hand, the larger the internal diameter of the pipeline (d), the higher the material consumption and production costs. On the other hand, the higher the internal diameter, the lower the hydraulic pressure loss and the operating costs of the electric motor. However, the Eq. (1) for investment costs (C_{inv}) published in [11] featured only the costs of the pipeline (C_{pipe}), i. e., equipment and its installation:

$$C_{inv} = C_{pipe} = B_0 \times d^{\chi} \times L \quad (1)$$

where B_0 and χ are empirical constants and L is the pipe length, m.

Operating costs (C_{oper}) were calculated as the energy consumption during operation times the price of kW per 1 h. The power required for pumping was defined as the volumetric flow rate (pump supply) multiplied by the pressure drop and divided by the pumping efficiency. However, the coefficient of hydraulic losses along the pipe length was calculated for new steel pipes with a turbulent flow, i. e., for hydraulically smooth pipes. The total annual costs were calculated as follows:

$$C = F \times C_{inv} + C_{oper} = C_0 + a_1 \times d + a_2/d^y \quad (2)$$

where F is the depreciation coefficient; C_0 stood for the costs unrelated to the pipeline diameter; a_1 and a_2 designated empirical constants; $a_1 \times d$ is the price of the pipeline; a_2/d^y is the energy costs for the pipeline; and y is an exponent that depended on the flow rate in the pipeline. By equating the derivative of function $C(d)$ to zero, Genereaux [11] found such diameter d_0 at which this function had a minimum. This approach was later adopted by numerous scientists.

Garcia & Steffe [12] were one of the first teams to report the optimal pipe diameter for transporting liquid food products. Their method was so successful that it was replicated worldwide. Garcia & Steffe rationalized the need to take into account the costs of the pumping station (C_{pump}): $C_{inv} = C_{pump} + C_{pipe}$. It included the price of the pump and engine, as well as their installation. Numerically, they expressed it as consumed power (N):

$$C_{pump} = B_1 + B_2 \times N^{\beta} \quad (3)$$

where B_1, B_2, and β are empirical constants.

As Garcia & Steffe [12] increased the value of N from 3 to 10 hp, the pumping station costs (C_{pump}) grew by only 1.8%. In fact, the dependence that Garcia & Steffe came up with in Eq. (3) was impossible to use in practical calculations because the cost of C_{pump} did not depend on the pipe diameter (Fig. 4).

Garcia & Steffe [12] used the Herschel–Bulkley rheological model to study the case of tomato ketchup transportation at a density of 1.110 kg/m^3 and a mass flow rate of 4 kg/s:

$$\tau = \tau_0 + K \times \omega^m; \mu = \tau_0/\omega + K \times \omega^{m-1} \quad (4)$$

where τ is the shear stress, Pa; τ_0 is the yield stress, Pa; K is the consistency index, Pa·s^m; m is the nondimensional flow rate; μ is the effective dynamic viscosity of fluid, Pa·s; and ω is the velocity shear, s^{-1}. The means obtained in [12] were as follows: τ_0 = 32 Pa; m = 0.27; K = 18.7 Pa·s^m.

The designed system consisted of 100 m of stainless-steel horizontal pipes with three 90° bends, a coupling, and two shut-off valves. The hydraulic pressure losses along pipe length (ΔP_L) was obtained specifically for this rheological model. As a result, the hydraulic pressure losses in local resistances $\Delta P_M = 0.5 \times \zeta \times \rho \times W^2$, with W being the fluid velocity in the pipe, were calculated for a turbulent flow. Cheese spread, however, is highly viscous, i. e., laminar.

Consumed power N was calculated conventionally [12]:

$$N = \Delta P \times Q/\eta; \Delta P = P_s + \Delta P_L + \Delta P_M \quad (5)$$

where η is the efficiency of the pipeline station (pipe + motor); ΔP is the pressure drop in the pump, Pa; P_s is the static pressure, Pa (0); and Q is the volumetric flow rate, m^3/s.

Garcia & Steffe [12] hypothesized that the efficiency was constant and had a quite high value (η = 0.7). Their calculations featured a rotary positive displacement pump, but they failed to specify its model and rotor speed n. The recommended rotor speed range for tomato ketchup was $n \approx$ 200–400 rpm. The effective dynamic viscosity of fluid, μ, for this rotor speed was 2.0–3.5 Pa·s (Eq. (4)). The efficiency of a rotary positive displacement pump dropped as the viscosity of the pumped liquid increased.

Naumov [13] attributed such a high efficiency to an Atlas W63-1B single-screw pump that pumped water at a pressure drop of ΔP = 0.6 MPa. While pumping jelly at the same pressure drop, the single-screw pump lost half of its efficiency, and efficiency η approximated 0.2 at ΔP = 0.2 MPa.

Factory tests of a food gear pump yielded a similar result. At a kinematic oil viscosity of 1,800 cSt, the maximal efficiency was η = 0.28 at a pressure drop of 0.6 MPa and η = 0.18 at ΔP = 0.2 MPa. The assumption that η = 0.7 = const [13] led to a double underestimation of the consumed power. The value of η could not be specified in advance since it depended on a number of factors determined by calculation. Finally, both [11] and [12] failed to specify the method used for determining F, i. e., coefficient corrects for wear and tear, in Eq. (2).

Other studies adopted the capital recovery ratio as F to evaluate investment projects. The ratio was calculated as follows:

$$F = \frac{r \times (1 + r)^k}{\left[(1 + r)^k - 1\right]^m} \quad (6)$$

where r is the precalculated interest rate and k is the time period. A combination of Generaux's method and Eq. (6) for the optimal pipeline diameter was named Life-Cycle Cost Analysis [14].

Some researchers attempted to optimize hydraulic calculations in food technology [15–18]. Arsana *et al*. [15] calculated the optimal diameter for a tube heat exchanger, favored by small food industry businesses. They applied a system of time-averaged Navier–Stokes equations to describe a stationary turbulent flow and heat exchange in the pipeline but reinforced this system with equations for pulsating energy and energy dissipation rate. This complex mathematical model made it possible to study the effect of the pipe diameter and inlet velocity on energy efficiency. However, Arsana *et al*. [15] failed to consider the fact that a smaller pipe diameter and a greater velocity could increase the hydraulic resistance, thus increasing the pressure and power requirements for the pump.

Khvostov *et al*. [16] calculated the optimal pipe diameter for transporting molasses as laminar liquid flow. Unfortunately, their calculations relied on a number of dubious assumptions:

– they took the local pressure loss coefficient as ζ = const, which is true only for turbulent flow;
– the pumping efficiency was assumed constant and was greatly overestimated (η = 0.8);
– the investment costs, which depended on the pipe diameter, did not include the price of the pump itself; and
– the rheological properties of the pumped liquid were not considered, and the pressure loss along the pipeline was calculated for a Newtonian liquid at μ = const.

In their later work [17], the same research team did adjust their pressure loss calculations for a non-Newtonian power-low liquid, but the first three assumptions persisted.

Golovanchikov *et al*. [18] compared optimal pipe diameter calculations for laminar, transitional, and turbulent flows. As for laminar flow, the required pump power depended inversely on d^4. However, the authors failed to consider the need to replace the pump when calculating different pipeline diameters. The resulting share of electricity costs was 96.8%.

All the abovementioned studies left out the load and energy characteristics of the pump in their attempts to optimize the pipeline unit. Garcia & Steffe [12] failed to provide a comprehensive assessment of the effect of pump cost on the optimal pipeline diameter because they used a pricelist with very similar prices. Moreover, they should have specified the pump type and model to take into account its characteristics. The choice of the pump type depends on the technological requirements. For instance, cheese spread production presupposes strict structure preservation measures and is likely to employ rotary lobe pumps. However, lobe pumps are very complex, expensive, and notorious for uneven supply.

The performance and energy efficiency of lobe pumps are another popular research topic [19–22]. Kang *et al*. [19] used the Navier–Stokes equations to study the effect of standard factors on lobe pumps. By reducing the gap size between rotor and casing wall from 1.25 to 0.5 mm, they quintupled the pressure. Pumps with three or four lobes demonstrated the same performance as two-lobe pumps but provided a more stable output. The clearance between two rotors could vary from 0.12 to 0.15 mm with no effect on pump performance.

Some publications report methods for reducing pressure fluctuations and liquid flow rate at the outlet of the lobe pump. Li *et al*. [20] developed a lobe pump with a gradually varied gap cavity. They also relied on the Navier–Stokes equation system for hydrodynamics. The authors claimed that the new design reduced the peak value of the pressure pulsation at the outlet that affected the rotor, thus weakening the effect of the rapid change of the outlet pressure on the radial exciting force.

Gans *et al*. [21] tested low-head lobe pumps at Chalmers University of Technology, Norway. The experimental lobe pump geometry consisted of a casing and two rectilinear three-lobe rotors with a cycloidal profile. The rotors were 3D-printed from acrylic. The numerical studies examined the curves related to the liquid pressure, rotation speed, and flow rate. The low rotation speed made it possible to avoid vibration.

Liu *et al*. [22] invented a noncircular gear variable speed drive that reduced the flow pulsation. They used numerical simulation to study the effect of different parameters of the noncircular gear, angular deviation, rotor-rotor gap, and input velocity on flow pulsations at the outlet. The Fourier noncircular gear made it possible to reduce pulsations by 84.1%. When the rotor-rotor gap was narrowed from 0.4 to 0.2 mm, the flow rate fluctuations dropped by 54.1%. Flow pulsation could be reduced by 60.0% when the input speed grew from 200 to 600 rpm.

Li *et al*. [23] studied the effect of fluid viscosity on the performance of the lobe pump. They pumped five different media with viscosity range from 1 to 110 cSt, both experimentally and in a numerical simulation. As the viscosity grew, the fluid flow in the cavity grew steady and hindered the leakage. The outlet flow rate of the 110 cSt medium was 40% higher than that with 1 cSt. As the rotation speed dropped from 400 to 100 rpm, the outlet flow rate decreased by 95% at 11 cSt and by 80% at 72 cSt. As a result, the gradient gap structure reduced pressure fluctuations by 30% in low-viscosity fluid.

While [19–23] featured the design stage, [24] and [25] focused on a different task. Many pump manufacturers make factory test results available to the public and provide all technical parameters for their pumps, e. g., correlation graphs for pump feed, power consumption, and rotor speed at different pressure drops. Akhmedova *et al*. [24, 25] developed a method for modeling the operating properties of a lobe pump based on the factory test data

published in technical documents. As effective dynamic viscosity μ of the pumped liquid increased, so did the pump supply and, to a larger extent, the consumed power. Therefore, the effect of low-viscosity food liquids on pump energy consumption was non-monotonic. The pump efficiency was maximal at a certain effective dynamic viscosity, which depended on the specific rotor speed and the pressure drop. No publications on optimal pipe diameter have featured this phenomenon so far.

In this research, we determined the optimal pipe diameter (d_0) for inter-operational transportation of food liquids with different viscosities at different lobe pump settings, as well as tested the effect of various factors on the method.

STUDY OBJECTS AND METHODS

The study featured a hydraulic system for transporting cheese spreads using a lobe pump. Table 1 illustrates the technical parameters and costs for different Russian brands of lobe pumps with a maximal pressure drop of 0.5 MPa.

As we see from Table 1, the cost of the pump increases by 63.3% as the electric motor power grows from 1.5 to 5.5 kW. This difference in pump costs is much greater than the one mentioned in [12]. Mind that the pump price depends more on its working volume (V_1) than on the nominal power of the electric motor (N_E). Publicly available price lists give similar data for lobe pumps. Figure 1 shows the effect of the working volume (V_1) on the pump cost (C_{pump}), and the resulting dependence is close to a linear function.

The cost of a pipe depends on its type. In this research, we used the price list posted on the website of PromTsvetMet LLC for AISI 304 EN10357 stainless-steel pipes with a wall thickness of 1.5 mm. In this abbreviation, EN10357 stands for the European Standard that features hygienic non-stainless-steel pipes for the food industry while AISI 304 means chromium-nickel steel. Such pipes neither oxidize nor react with the food environment. In addition, they are resistant to decay, fungus, and mold.

Figure 2 illustrates the effect of the internal diameter on the costs of these pipes. The resulting dependence is close to a linear function:

$$C_{pipe} = B_0 \times d \times L = \Psi(d) \times L \quad (7)$$

where the coefficient in B_0 is the 19 thousand rubles per 1 m^2; d is the internal diameter, m; and L is the pipe length, m.

If technological requirements presuppose a thicker wall, the cost of the pipes increases, and so does empirical coefficient B_0 in Eq. (7).

To calculate such operating characteristics as supply and consumed power, we used the method described in [24, 25]:

$$Q = \Psi_1(n, p, \mu b) = V_1 \times n - B_1 \times p \times \mu b^{-\alpha} \quad (8)$$

$$N = \Psi_2(n, p, \mu b) = n \times (a_0 + a_1 \times p + a_2 \times \mu b) \quad (9)$$

where V_1 is the volume pumped in one revolution ($\Delta P = 0$), L; $\mu b = \mu/\mu_0$ is the nondimensional effective dynamic

Table 1 Lobe pump brands: Technical parameters and costs (public sources)

Brand	Pump working volume (V_1), L	Flow rate (Q), m^3/h	Nominal power of electric motor (N_E), kW	Pump cost (C_{pump}), thousand rubles
KN-015	0.15	1.8–5.0	1.5	278.0
			2.2	282.8
KN-032	0.32	1.0–7.0	3.0	313.0
			4.0	316.8
KN-070	0.70	2.5–17.0	4.0	438.8
			5.5	454.1

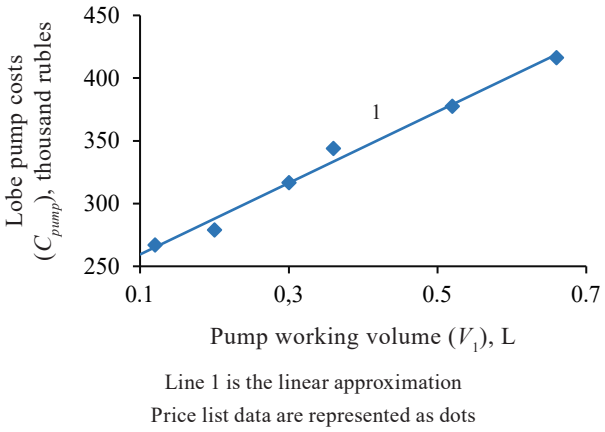

Figure 1 Lobe pump costs vs. pump working volume

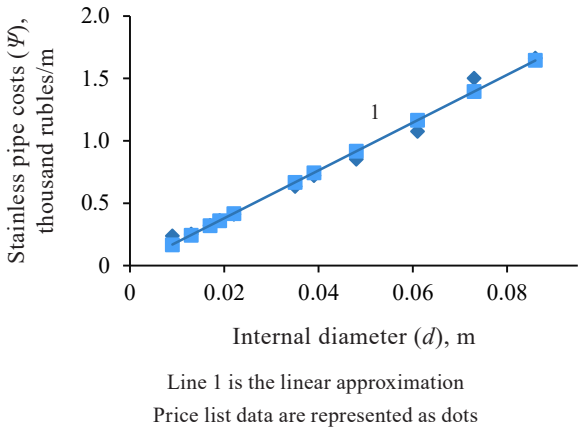

Figure 2 Effect of internal diameter on stainless pipe costs

viscosity of fluid; μ_0 is the dynamic viscosity of water at 20°C, Pa·s; $p = \Delta P/P_A$ is the nondimensional pressure drop; P_A is the atmospheric pressure, Pa; and B_1, α, a_0, a_1, a_2 are empirical constants.

Figures 3 and 4 show examples of how supply and consumed power in a KNP-30 lobe pump depend on the pressure drop, calculated in line with Eq. (8) and (9) for different effective dynamic viscosities. The greater the effective dynamic viscosity of the pumped fluid, the less the difference between the actual supply and its theoretical value $Q_T = V_1 \cdot n$. The consumed power rises while the efficiency falls.

The effective dynamic viscosity of food products depends on their composition, temperature (T, °C) and shear rate (ω, s^{-1}). Some rheological studies of cheese spreads [26–28] described the change in effective dynamic viscosity using the Ostwald–de Waele model for power-law fluid:

$$\mu = K \times \omega^{m-1} \quad (10)$$

Cheese spreads are supplied at high temperatures, which means we were able to use the results that we had reported in [25] for seven different cheese spread samples at T = 55–95°C. Table 2 shows the composition of three cheese spreads we described in [25].

According to [25] and [26], the effect of temperature on consistency index K and nondimensional flow rate m was calculated as follows:

$$K = K_0 \times T^{\beta}, m = m_0 + \gamma \times T \quad (11)$$

where K_0, β, m_0, and γ are the empirical constants obtained by the least-square method for each cheese spread sample.

For each specific cheese spread sample, the nondimensional effective dynamic viscosity depended on the temperature and rotor speed:

$$\mu b(T, n) = K(T) \times (2 \times \pi \times n)^{m(T)-1} \quad (12)$$

The pressure losses caused by friction along the pipeline was calculated using the Darcy–Weisbach equation [12]:

$$\Delta P_L = 0.5 \times \lambda \times \rho \times (L/\mathrm{d}) \times W^2 \quad (13)$$

where L is the pipe length, m; d is the internal diameter of the pipeline, m; W is the mean velocity of liquid in the pipeline for cross section, m/s; ρ is the liquid density, kg/m^3; and λ is the coefficient of loss caused by friction along the pipeline.

Csizmadia & Till [29] and Bibok *et al.* [30] calculated the loss coefficient for non-Newtonian power-low laminar liquid as $\lambda = 64/\mathrm{Re}_{PL}$ using a modified Raynolds factor:

$$\mathrm{Re}_{PL} = \frac{W^{2-m} \times d^m \times \rho}{8^{m-1} \times K \times \left(\frac{3 \times m + 1}{4 \times m}\right)^m} \quad (14)$$

Unlike Garcia & Steffe [12] and Khvostov *et al.* [16], we took into account the dependence of ζ on the Reynolds

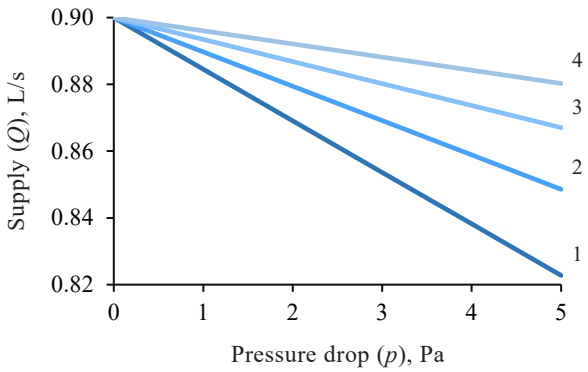

Figure 3 Effect of pressure drop on supply at n = 3 s^{-1} and different effective dynamic viscosities: 1 – μb = 50; 2 – μb = 150; 3 – μb = 500; and 4 – μb = 2,000

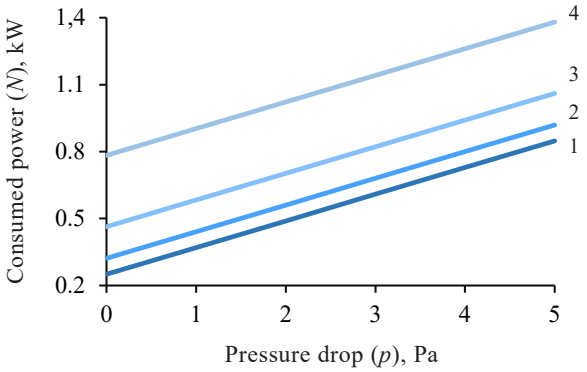

Figure 4 Effect of pressure drop on consumed power at n = 3 s^{-1} and different effective dynamic viscosities: 1 – μb = 50; 2 – μb = 150; 3 – μb = 500; and 4 – μb = 2,000

Table 2. Cheese spreads: Composition [25]

Sample	Gouda cheese, %	Water, %	Butter, %	Skimmed milk powder, %	Sodium citrate, %
1 (1)*	50.5	37.5	0	9.0	3.0
2 (6)*	43.0	24.5	27.0	2.5	3.0
3 (7)*	60.0	17.0	17.5	2.5	3.0

* – as labeled in [25]

factor in the power-law laminar fluid to calculate the pressure loss in local hydraulic resistances:

$$\Delta P_M = 0.5 \times \zeta \times \rho \times W^2; \zeta = \Theta / Re_{PL} \quad (15)$$

where Θ is the nondimensional coefficient that depended on the type of local hydraulic resistance and its nondimensional parameters.

Equation (15) was tested in [29, 30] for power-law laminar fluid in a circular pipe, and Θ proved to depend on pipeline curvature radius (R) in the elbow: Θ was 180 at $R = d$ and approximated 400–650 at $R = d/2$.

By using Eq. (12)–(14) in Eq. (16), we calculated φ, i. e., the effect of volumetric flow rate (Q) on pressure drop (ΔP) at a given temperature (T):

$$\varphi(Q) = P_C + 2^{3m-4} \times K \times \times \left(\frac{3 \times m + 1}{4 \times m} \times \frac{4 \times Q}{\pi \times d^3}\right)^m \times \left(64 \times \frac{L}{d} + \Sigma\Theta\right) \quad (16)$$

We calculated rotor speed (n_0) required to provide a specific value of Q_0 at a specific point in the pumping unit:

$$\Psi_1(n_0, \varphi(Q_0, d_i)/P_A; \mu b(n_0, T)) = Q_0 \quad (17)$$

Equation (17) was solved numerically for a series of given diameter values (d_i) to calculate the corresponding series (n_{0i}). This series made it possible to calculate the power values for the lobe pump:

$$N_i = \Psi_2(n_{0i}, \varphi(Q_0)/P_A; \mu b(n_{0i}, T))) \quad (18)$$

Power N consumed by the electric pump unit was necessary to calculate the annual electricity costs:

$$C_{oper} = z \times A_E = z \times N \times t; t = t_0 \times Y \quad (19)$$

where z is the electricity tariff, thousand rubles per kW/h; A_E is the work, kW·h, expended by the pump electric motor per time period (t, h); t_0 is the number of hours the lobe pump worked per day; and Y is the number of working days per year. In our research, we determined N directly by the energy characteristic of a specific pump Eq. (9), not by hydraulic power as in [12, 16–18].

Equation (19) cannot work without a particular z, i. e., the cost of electric power. Electricity prices vary from region to region and tend to increase. In this research, we used electricity prices for particular small businesses from three random regions valid as of June 2024:

– Rusenergosbyt LLC, z_1 = 3.6697 rubles/kW·h (Irkutsk Region);

– Kuzbassenergosbyt Ltd, z_2 = 7.1462 rubles/kW·h (Kemerovo Region);

– RKS Energiya Ltd, z_3 = 10.658 rubles/kW·h (Leningrad Region).

The share of the total costs that depends on the pipe diameter was represented as a sum for every pump number (j) in line:

$$C_j = F(r, k) \times (CP_j + B_0 \times \cdot d \times L + z \times N_j \times t_0 \times Y) \quad (20)$$

where CP_j is the price of every j^{th} pump.

Consumed power (N) was a decreasing function of the diameter (Fig. 5b), and the derivative of this function was negative.

By finding $C'(d) = 0$, we calculated the most economical diameter (d_{0j}) for every pump number (j) in line. The next step was to choose the value in the d_{0j} series that provided the lowest cost in Eq. (20) based on the restrictions imposed on the rotor speed by high viscosity liquids.

RESULTS AND DISCUSSION

Our calculations were performed under the following conditions: Q_0 = 1.2 L/s; $z = z_2$ = 7.1462 rubles/kW·h; L = 30 m; ΣΘ = 3,000; P_s = 500 kPa; r = 0.1; k = 10; and t_0 = 8 h. Sample 1 was transported at T = 85°C. Not to damage its structure, the rotor speed was limited to $n \leq 250$ rpm.

Below, we used the working characteristics of the KNP-30 lobe pump model (Fig. 3 and 4). Figure 5a shows the numerical solution of Eq. (17), i. e., the values of rotor speed (n_0) that provide flow rate (Q_0) in the given hydraulic system. Figure 5b shows the power of the KNP-30 lobe pump calculated using Eq. (18).

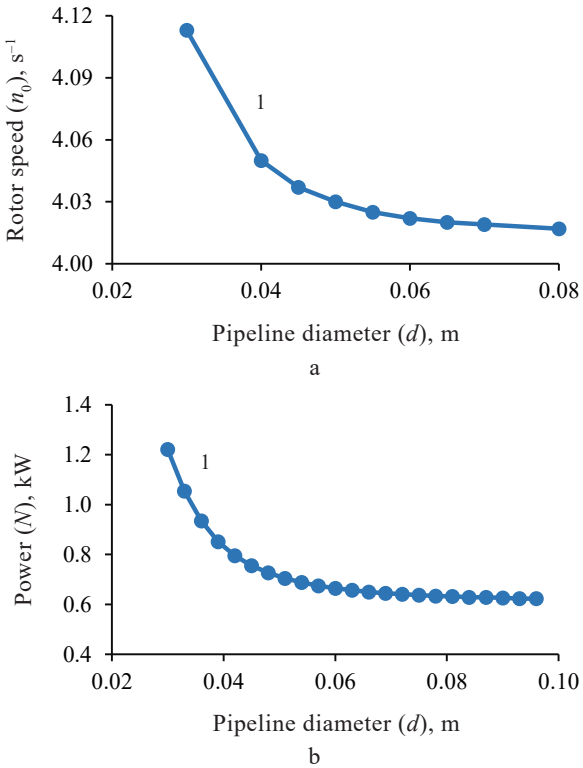

Dots – calculation results; Lines – approximations

Figure 5 Parameters of KNP-30 pump at flow rate Q_0 = 1.2 L/s and specified pipeline diameter: (a) rotor speed; (b) power

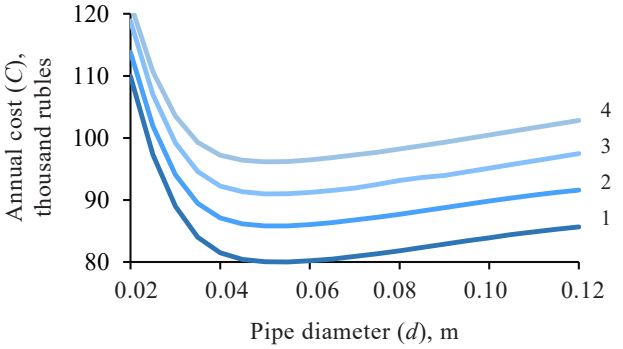

Figure 6 Effect of pipe diameter on reduced annual cost at Q_0=1.2 L/s, t_0=8 h for different pump models: 1 – KNP-20; 2 – KNP-30; 3 – KNP-36; and 4 – KNP-52

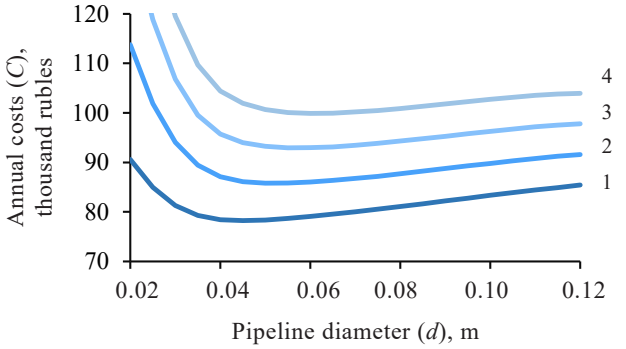

Figure 7 Effect of pipeline diameter and daily operation time t_0 on reduced annual costs for KNP-30 at Q_0 = 1.2 L/s: 1 – t_0 = 4 h; 2 – t_0 = 8 h; 3 – t_0 = 12 h; and 4 – t_0 =16 h

Table 3 Optimal pipe diameter and other parameters at Q_0 = 1.2 L/s at t_0 = 8 h for different pump models

Mump model	Optimal pipe diameter (d_0), mm	Rotor speed (n_0), s^{-1}	Reduced annual costs (C), thousand rubles	Pump pressure drop (ΔP), kPa	Consumed power (N), kW	Efficiency (η)
KNP-20	53.0	6.03	80.01	98.4	0.788	0.150
KNP-30	52.2	4.03	85.78	101.0	0.698	0.174
KNP-36	52.0	3.36	90.94	101.4	0.678	0.179
KNP-52	51.1	2.33	96.14	105.0	0.602	0.209

Table 4 Optimal pipe diameter and other parameters for KNP-30 at Q_0 = 1.2 L/s and different daily operation times

Daily operation time (t_0), h	Optimal pipe diameter (d_0), mm	Rotor speed (n_0), s^{-1}	Reduced annual costs (C), thousand rubles	Pump pressure drop (ΔP), kPa	Consumed power (N), kW	Efficiency (η)
4	44.6	4.038	78.25	138.5	0.760	0.219
8	52.2	4.028	85.78	101.0	0.698	0.174
12	57.1	4.024	92.93	87.3	0.675	0.155
16	60.9	4.022	99.90	79.8	0.663	0.145

According to Fig. 5b, the consumed power strongly depended on the diameter. The number in the model corresponded to the theoretical volume of liquid pumped in 100 revolutions (V_1, L). For KNP-30, pump working volume (V_1) equaled 0.30 L. The numerical value of rotor speed Q_0/V_1 equaled 1.2/0.3 = 4.0 s^{-1}. The target rotor speed exceeded the numerical value by only a few percent due to the high viscosity of cheese spread and the relatively small pressure drop.

Knowing consumed power (N), we could use Eq. (20) to calculate the reduced annual costs for KNP-30 and other lobe pumps (Fig. 6). All graphs had a minimum that corresponded to the most economical diameter for each model. The lower V_1, the lower the reduced annual costs, considering the limited rotor speed.

Table 3 shows the numerical values of the optimal diameter for several lobe pump models, as well as reduced costs, pressure drop, consumed power, efficiency, and rotor speed at a particular diameter. Model KNP-20 demonstrated the lowest reduced costs, but its rotor speed was n_0 = 6.03 s^{-1} = 361.8 rpm, which exceeded the permissible value. This requirement was met for KNP-30: n_0 = 4.03 s^{-1} = 241.8 rpm < 250 rpm. The obtained results mean that the KNP-30 lobe pump model demonstrated the best industrial potential. The optimal diameter decreased insignificantly with increasing V_1. The pipe was selected from actual models mentioned in an official catalogue. A stainless-steel pipe of 63.5×1.5×6,000 had an internal diameter of 47.5 mm, which was below the value precalculated for d_0. A stainless-steel pipe of 76.1×1.5×6,000 had an internal diameter of 73.1 mm, which was too big.

According to Table 3, the efficiency increased from 0.150 to 0.209. If we had assumed η = const, as in previous studies, the calculation results would have been distorted.

Below, we examined the effect of various factors on the reduced annual costs and the optimal pipe diameter. Figure 7 illustrates the effect of daily operation time on the reduced annual costs for the KNP-30 pump model.

Table 4 shows the optimal pipe diameter and other parameters for the KNP-30 pump model at different daily operation times (t_0).

As the operating time grew, the share of costs for electric energy increased. As a result, the optimal diameter increased significantly to reduce the hydraulic pressure losses, pump pressure drop, and energy costs. The

Table 5 Optimal pipe diameter and other parameters for KNP-30 at t_0 = 8 h and Q_0 = 1.2 L/s for different electricity tariffs

Electricity tariff (z), rubles/kW·h	Optimal pipe diameter (d_0), mm	Rotor speed (n_0), s^{-1}	Reduced annual costs (C), thousand rubles	Pump pressure drop (ΔP), kPa	Consumed power (N), kW	Efficiency (η)
3.6697	44.9	4.037	78.47	136.5	0.757	0.217
7.1462	52.2	4.028	85.78	101.0	0.698	0.174
10.6580	57.0	4.024	92.81	87.4	0.675	0.155
15.0000	61.5	4.022	101.27	78.7	0.661	0.143

Table 6 Optimal pipe diameter and other parameters for KNP-30 at t_0 = 8 h and Q_0 = 1.2 L/s for different pipe lengths

Pipe lengths (L), m	Optimal pipe diameter (d_0), mm	Rotor speed (n_0), s^{-1}	Reduced annual costs (C), thousand rubles	Pump pressure drop (ΔP), kPa	Consumed power (N), kW	Efficiency (η)
10	53.4	4.019	80.59	68.1	0.643	0.127
30	52.2	4.028	85.78	101.0	0.698	0.174
60	52.0	4.041	93.56	149.7	0.778	0.231
120	51.9	4.067	109.16	245.7	0.939	0.314

Table 7 Optimal pipe diameter and other parameters for KNP-30 at t_0 = 8 h and Q_0 = 1.2 L/s at different static pressures

Static pressure (P_s), MPa	Optimal pipe diameter (d_0), mm	Rotor speed (n_0), s^{-1}	Reduced annual costs (C), thousand rubles	Pump pressure drop (ΔP), kPa	Consumed power (N), kW	Efficiency (η)
0	52.1	4.014	84.06	51.2	0.615	0.100
0.05	52.2	4.028	85.78	101.0	0.698	0.174
0.10	52.3	4.041	87.51	150.7	0.780	0.232
0.20	52.5	4.069	91.02	250.2	0.947	0.317

Table 8 Optimal pipe diameter and other parameters for KNP-30 at t_0 = 8 h and Q_0 = 1.2 L/s at different temperatures

Temperature (T), °C	Optimal pipe diameter (d_0), mm	Rotor speed (n_0), s^{-1}	Reduced annual costs (C), thousand rubles	Pump pressure drop (ΔP), kPa	Consumed power (N), kW	Efficiency (η)
65	72.9	4.019	96.53	123.6	1.095	0.135
75	60.8	4.023	89.89	110.5	0.846	0.157
85	52.2	4.028	85.78	101.0	0.698	0.174
95	45.8	4.033	83.07	94.2	0.604	0.187

reduced costs increased, the efficiency went down, and the rotor speed remained practically the same.

Table 5 shows the optimal pipe diameter and other parameters for KNP-30 at different electricity tariffs z. As electricity tariffs grew, so did the operating costs. Therefore, a larger optimal diameter made it possible to reduce the pressure losses along the pipeline. As a result, the reduced costs increased while the pressure drop and the consumed power decreased.

Table 6 gives the optimal pipe diameter and other parameters for the KNP-30 pump model at different pipeline lengths (L). As the pipeline length increased from 10 to 120 m, the reduced costs grew from 80.59 to 109.16 thousand rubles and the consumed power increased from 0.643 to 0.939 kW while the optimal diameter decreased by 1.5 mm.

Table 7 shows the optimal pipe diameter and other parameters for KNP-30 at different static pressures (P_s). As the static pressure grew from 0 to 0.2 MPa, the reduced costs rose from 84.06 to 91.02 thousand rubles while the consumed power increased from 0.615 to 0.947 kW. The optimal pipe diameter increased insignificantly, by only 0.4 mm.

Table 8 shows the optimal pipe diameter and other parameters for KNP-30 at different temperatures (T). As the temperature grew, the effective dynamic viscosity and consumed power went down. As a result, the optimal diameter and reduced costs dropped while the efficiency increased. For instance, as the temperature of cheese spread in Sample 1 rose from 65 to 95°C, the optimal pipe diameter decreased from 72.9 to 45.8 mm.

Table 9 shows the optimal pipe diameter and other parameters for KNP-30 at different flow rates.

As the flow rate grew, so did the hydraulic pressure losses and the costs of electric energy. As a result, the optimal pipe diameter increased significantly to reduce ΔP and energy costs. The efficiency decreased while the reduced costs and the rotor speed increased. Moreover, the rotor speed started to exceed the permissible value of 4.167 s^{-1} as early as at Q_0 = 1.6 L/s. Therefore, KNP-52 proved to be more effective for the two bottom flow rates in Table 9.

Table 10 shows the optimal pipe diameter and other parameters for KNP-52 and different cheese spreads. Across Samples 1–3, the effective dynamic viscosity increased at the same temperature and rotor speed. As a result, pumping required more energy costs for Sample 3 than for Sample 1. The optimal pipe diameter had to increase from 53.5 to 84.5 mm to partially compensate for this effect. Nevertheless, the reduced costs rose from 99.22 to 118.6 thousand rubles.

Table 11 illustrates the optimal pipe diameter and other parameters for KNP-52 at different Life-Cycle values (k).

Table 12 demonstrates the same values for different interest rates (r). As the Life-Cycle value increased, the optimal pipe diameter increased, i. e., the reduced costs went down. As the interest rate grew, the optimal pipe diameter decreased, i. e., the reduced costs went up.

CONCLUSION

In this research, we developed a new method for determining optimal pipe diameter (d_0) for inter-operational transportation of food liquids based on their viscosity and lobe pump properties. The method consisted of the following stages:

1. We analyzed the prices for lobe pumps and pipes to obtain an analytical dependence of the pipe costs on internal diameter (d) as in Eq. (7).

2. Having used the available technical documentation, we calculated the effect of rotor speed, pressure drop, and viscosity on performance and power of the lobe pump as in Eq. (8) and (9).

3. We used experimentally obtained data to reveal the effect of velocity shift and temperature on the dynamic viscosity of the pumped liquid as in Eq. (11) and (12) for the power-law liquid model, although other rheological models are possible.

4. To determine the characteristics of the process pipeline, we studied the static pressure, as well as the effect of liquid flow rate (Q) and internal diameter (d) on pressure loss along the pipe length and local hydraulic losses as in Eq. (16).

Table 9 Optimal pipe diameter and other parameters for KNP-30 at t_0 = 8 h and different flow rates

Flow rate (Q_0), L/s	Optimal pipe diameter (d_0), mm	Rotor speed (n_0), s^{-1}	Reduced annual costs (C), thousand rubles	Pump pressure drop (ΔP), kPa	Consumed power (N), kW	Efficiency (η)
0.8	44.1	2.698	80.03	114.9	0.468	0.196
1.2	52.2	4.028	85.78	101.0	0.698	0.174
1.6	58.7	5.359	91.68	93.4	0.944	0.158
2.0	64.3	6.692	97.83	88.3	1.207	0.146

Table 10 Optimal pipe diameter and other parameters for KNP-52 at t_0 = 8 h and Q_0 = 1.6 L/s for various cheese spread samples

Cheese spread sample	Optimal pipe diameter (d_0), mm	Rotor speed (n_0), s^{-1}	Reduced annual costs (C), thousand rubles	Pump pressure drop (ΔP), kPa	Consumed power (N), kW	Efficiency (η)
1	53.5	3.106	99.22	93.8	0.736	0.204
2	60.7	3.101	104.63	109.1	0.954	0.183
3	84.5	3.095	118.60	134.3	1.489	0.144

Table 11 Optimal pipe diameter and other parameters for KNP-52 at t_0 = 8 h, Q_0 = 1.6 L/s, and r = 0.1 for different Life-Cycle values

Life-Cycle values (k)	Optimal pipe diameter (d_0), mm	Rotor speed (n_0), s^{-1}	Reduced annual costs (C), thousand rubles	Pump pressure drop (ΔP), kPa	Consumed power (N), kW	Efficiency (η)
4	54.5	3.105	149.81	131.4	0.998	0.211
7	60.7	3.101	104.63	109.1	0.954	0.183
10	64.3	3.098	86.99	99.8	0.936	0.171
15	67.8	3.097	74.01	92.5	0.922	0.161

Table 12 Optimal pipe diameter and other parameters for KNP-52 at t_0 = 8 h, Q_0 = 1.6 L/s, and k = 7 for different interest rates

Interest rate (r)	Optimal pipe diameter (d_0), mm	Rotor speed (n_0), s^{-1}	Reduced annual costs (C), thousand rubles	Pump pressure drop (ΔP), kPa	Consumed power (N), kW	Efficiency (η)
0.05	63.3	3.099	91.16	102.0	0.940	0.174
0.07	62.3	3.100	96.43	104.8	0.946	0.177
0.10	60.7	3.101	104.63	109.1	0.954	0.183
0.15	58.4	3.102	119.02	116.4	0.968	0.192

5. To define rotor speed (n_0) able to provide a target value of Q_0 at a specific operating point, we applied Eq. (17) to several internal diameters and used Eq. (18) to calculate the corresponding consumed power values.

6. Equation (20) made it possible to form target function $C_j(d)$ for the reduced annual costs that depended on the pipeline diameter for each j^{th} pump.

7. Equation $C'(d) = 0$ revealed the most economically rational diameter (d_{0j}) for every j^{th} pump. The last step was to select the value that provided the lowest costs in Eq. (20), based on the rotor speed limitations related to high-viscosity liquids.

Of all factors affecting optimal pipe diameter (d_0), the biggest impact belonged to the viscosity of the pumped liquid, which, in its turn, depended on the temperature. As the temperature of the cheese spread increased from 65 to 95°C, the optimal diameter dropped from 72.9 to 45.8 mm and the reduced annual costs decreased by 14%.

As the operation time grew, the electricity costs increased, resulting in a larger optimal diameter to reduce the hydraulic pressure losses, pump pressure drop (ΔP), and energy costs. The reduced costs increased while the pump efficiency decreased.

Higher electricity tariffs increased the operating costs. As a result, the optimal pipe diameter increased to reduce the pressure losses along the pipeline. Subsequently, the reduced annual costs increased while the pressure and the consumed power went down.

The optimal diameter grew significantly together with the liquid flow while the efficiency decreased and the reduced annual costs and rotor speed grew.

A higher static pressure and pipeline length correlated with much higher reduced annual costs while the optimal pipe diameter remained almost the same.

The optimal pipe diameter depended on the investment parameters. Bigger Life-Cycle values correlated with bigger optimal diameters, which means that the reduced annual costs decreased. Higher interest rates reduced the optimal pipe diameter, thus raising the reduced costs.

The efficiency of the pipe station depended on all the factors investigated in this research, which means that the assumption of η = const adopted in other studies provided false results.

CONTRIBUTION

The authors were equally involved in the research and are equally responsible for any potential plagiarism.

CONFLICT OF INTEREST

The authors declared no conflict of interest regarding the publication of this article.

REFERENCES

1. Mohamed AG, Ibrahim OAEH, Gafour WAMS, Farahat ESA. Comparative study of processed cheese produced from sheep and cow milk. Journal of Food Processing and Preservation. 2021;45(1):e15003. https://doi.org/10.1111/jfpp.15003
2. Salunke P, Biswas AC, Metzger LE. Manufacture of loaf-type processed cheese products using transglutaminase crosslinked micellar casein concentrate and milk protein concentrate. International Journal of Dairy Technology. 2023;76(4):727–736. https://doi.org/10.1111/1471-0307.12977
3. Irfan S, Murtaza MA, Din GM, Hafiz I, Murtaza MS, *et al*. Physicochemical, microbial, and functional attributes of processed Cheddar cheese fortified with olive oil–whey protein isolate emulsion. Food Science & Nutrition. 2023;11(3):1247–1256. https://doi.org/10.1002/fsn3.3159
4. Kratochvílova A, Salek RN, Vašina M, Lorencová E, Kůrová V, *et al*. The impact of different hydrocolloids on the viscoelastic properties and microstructure of processed cheese manufactured without emulsifying salts in relation to storage time. Foods. 2022;11(22):3605. https://doi.org/10.3390/foods11223605
5. Saraiva BR, Cegudo ACM, Gibin MS, Silva JB, Sato F, *et al*. Co-product from debittering process of trub (brewing by-product) as natural antioxidant in processed cheese. International Journal of Food Science and Technology. 2023;58(12):6752–6760. https://doi.org/10.1111/ijfs.16643
6. Maytakov AL, Yusupov ST, Popov AM, Kravchenko SN, Bakin IA. Study of the process of concentration as a factor of product quality formation. Foods and Raw Materials. 2018;6(1):172–181. https://doi.org/10.21603/2308-4057-2018-1-172-181
7. Zhang Y, Munir MT, Udugama I, Yu W, Young BR. Modelling of a milk powder falling film evaporator for predicting process trends and comparison of energy consumption. Journal of Food Engineering. 2018;225:26–33. https://doi.org/10.1016/j.jfoodeng.2018.01.016
8. Hettiarachchi CA, Harte FM, Voronin GL. Spray drying of high pressure jet-processed condensed skim milk. Journal of Food Engineering. 2019;261:1–8. https://doi.org/10.1016/j.jfoodeng.2019.04.007
9. Plotnikov KB, Popov AM, Plotnikov IB, Kryuk RV, *et al*. Improving the line of instant starch soft drinks. Food Processing: Techniques and Technology. 2020;50(1):96–105. (In Russ.) https://doi.org/10.21603/2074-9414-2020-1-96-105
10. Stoforos GN, Simunovic J. Computer-aided design and experimental testing of continuous flow cooling of viscous foods. Journal of Food Process Engineering. 2018;41(8):e12913. https://doi.org/10.1111/jfpe.12913
11. Genereaux RP. Fluid-flow design methods. Industrial & Engineering Chemistry. 1937;29(4):385–388. https://doi.org/10.1021/ie50328a007

12. Garcia EJ, Steffe JF. Optimum economic pipe diameter for pumping Herschel-Bulkley fluids in laminar flow. Journal of Food Engineering. 1986;8(2):117–136. https://doi.org/10.1111/j.1745-4530.1986.tb00105.x
13. Naumov VA. Effect of liquid food viscosity on the load characteristics of single-screw pumps. Food Processing: Techniques and Technology. 2021;51(2):290–300. (In Russ.) https://doi.org/10.21603/2074-9414-2021-2-290-300
14. Arumugam A, Habtay G, Kibrom H, Gebreamlak M. Comparison of optimal pipe sizing designs for pressurized flow system. International Journal of Computer Sciences and Engineering. 2018;6(8):520–529. https://doi.org/10.26438/ijcse/v6i8.520529
15. Arsana IM, Putra YRR, Sari HN, Nurjannah I, Wahyuono RA. Optimized hydraulic diameter and operating condition of tube heat exchanger for food industry – A numerical study. Journal of Mechanical Engineering Research and Developments. 2020;43(6):329–338.
16. Khvostov AA, Magomedov MG, Zhuravlev AA, Shipilova EA, Semenikhin OA, *et al*. Optimization of process pipeline parameters by techno-economic parameters. Proceedings of Voronezh State University of Engineering Technologies. 2020;82(1):34–46. (In Russ.) https://elibrary.ru/RMJPHT
17. Khvostov AA, Ivanov AV, Zhuravlev AA. Optimization of pipeline parameters for transportation liquid media with a viscosity anomaly. Information technologies in construction, social and economic systems. 2020;(2):18–22. (In Russ.) https://elibrary.ru/YSLPXI
18. Golovanchikov AB, Dulkin TA, Prokhorenko NA, Merentsov NA. Optimization of technological parameters and diameter of the pipeline, taking into account energy and resource conservation. Transactions TSTU. 2020;26(1):91–99. (In Russ.) https://doi.org/10.17277/vestnik.2020.01.pp.091-099
19. Kang YH, Vu HH, Hsu CH. Factors impacting on performance of lobe pumps: A numerical evaluation. Journal of Mechanics. 2012;28(2):229–238. https://doi.org/10.1017/jmech.2012.26
20. Li YB, Guo DS, Li XB. Mitigation of radial exciting force of rotary lobe pump by gradually varied gap. Engineering Applications of Computational Fluid Mechanics. 2018;12(1):711–723. https://doi.org/10.1080/19942060.2018.1517053
21. Gans LHA, Trivedi C, Iliev I, Storli PT. An experimental and numerical study of a three-lobe pump for pumped hydro storage applications. Journal of Physics: Conference Series. 2023;2629:012010. https://doi.org/10.1088/1742-6596/2629/1/012010
22. Liu D, Xu C, Shi L, Tian B, Jin X. Flow fluctuation abatement method and flow characteristics of lobe pump by external noncircular gear drive. Journal of Mechanical Science and Technology. 2024;38:271–284. https://doi.org/10.1007/s12206-023-1223-x
23. Li YB, Du J, Guo DS. Numerical research on viscous oil flow characteristics inside the rotor cavity of rotary lobe pump. Journal of the Brazilian Society of Mechanical Sciences and Engineering. 2019;41:274. https://doi.org/10.1007/s40430-019-1781-0
24. Akhmedova NR, Levicheva OI, Naumov VA. Influence of liquid food products viscosity on lobe pump performance (case of pumping fish oil). Vestnik of Astrakhan State Technical University. Series: Fishing Industry. 2022:(3):74–81. https://doi.org/10.24143/2073-5529-2022-3-74-81
25. Akhmedova NR, Levicheva OI, Naumov VA. Influence of liquid food products viscosity on the lobe pump energy efficiency. Izvestiya vuzov. Food Technology. 2023;(5–6):83–93. (In Russ.) https://doi.org/10.26297/0579-3009.2023.5-6.14
26. Dimitreli G, Thomareis AS. Effect of temperature and chemical composition on processed cheese apparent viscosity. Journal of Food Engineering. 2004;64(2):265–271. https://doi.org/10.1016/j.jfoodeng.2003.10.008
27. Pluta-Kubica A, Černíková M, Dimitreli G, Nebesářová J, Exarhopoulos S, *et al*. Influence of the melt holding time on fat droplet size and the viscoelastic properties of model spreadable processed cheeses with different compositions. International Dairy Journal. 2021;113(2):104880. https://doi.org/10.1016/j.idairyj.2020.104880
28. Šantová K, Salek RN, Kůrová V, Mizera A, Lapčíková B, *et al*. Potassium-based emulsifying salts in processed cheese: A rheological, textural, tribological and thermal approach. Journal of Dairy Science. 2024;107(10):7704–7717. https://doi.org/10.3168/jds.2024-24939
29. Csizmadia P, Till S. The effect of rheology model of an activated sludge on to the predicted losses by an elbow. Periodica Polytechnica Mechanical Engineering. 2018;62(4):305–311. https://doi.org/10.3311/PPme.12348
30. Bíbok M, Csizmadia P, Till S. Experimental and numerical investigation of the loss coefficient of a 90° pipe bend for power-law fluid. Periodica Polytechnica Chemical Engineering. 2020;64(4):469–478. https://doi.org/10.3311/PPch.14346

Additional information about the authors

Natalya R. Akhmedova ORCID 0000-0003-3483-3580; eLIBRARY SPIN 5896-2408
Oksana I. Levicheva ORCID 0000-0001-5922-9123; eLIBRARY SPIN 3957-5290
Vladimir A. Naumov ORCID 0000-0003-0560-5933; eLIBRARY SPIN 1788-8843